Room temperature continuous wave, monolithic tunable THz sources based on highly efficient mid-infrared quantum cascade lasers

Quanyong Lu, Donghai Wu, Saumya Sengupta, Steven Slivken, & Manijeh Razeghi*

Center for Quantum Devices, Department of Electrical Engineering and Computer Science, Northwestern University, Evanston, IL 60208, USA. *razeghi@eecs.northwestern.edu

Supplementary Material

1. Calculation of the nonlinear susceptibility $\chi^{(2)}$ for strain-balanced active region design

Coupling strength ħΩ between the injector level 4 and upper lasing level 5 governs the resonant current density *J*, as seen from the following equation[1, 23]:

$$J = eN_s \frac{2\Omega^2 \tau_\perp}{1 + \Delta^2 \tau_\perp^2 + 4\Omega^2 \tau_{ul} \tau_\perp} \qquad (1)$$

where N_s is the sheet doping density, ħΔ is the energy detuning of tunnelling transition, τ_{ul} is the upper level transition time to the lower level, $\tau_\perp$ is the momentum relaxation time in the quantum well plane. The coupling should be strong enough for efficient carrier injection to the upper level and less susceptibility to the energy detuning to the resonance tunnelling condition, yet it should not exceed the transition broadening to avoid the splitting of the gain.

In the present strain-balanced material system with a diagonal-transition active region design, the increased conduction-band offset and interface roughness increases the broadening of the transition linewidth to 15-20 meV, compared to that of ~10 meV for the lattice-matched active region design. This allows for a stronger coupling design between the injector and upper lasing level. A high coupling strength with an energy splitting of $2\hbar\Omega$ =16.5 meV is used in current design.

The strong-coupled strain-balanced design brings two type schemes contributing to the DFG nonlinear susceptibility $\chi^{(2)}$ which involves the strong coupling between lower laser levels 1, 2, and 3 (Fig. 1(b)), and the strong coupling between the upper laser levels 4 and 5 (Fig. 1(c)). Therefore, $\chi^{(2)}$ is rewritten as[29]:

$$\begin{aligned}
&\chi^{(2)}\left(\omega_{THz}=\omega_1-\omega_2\right)\approx \\
&\frac{e^3}{\hbar^2\varepsilon_0}\sum_{j,k=1,2,3;\,j\neq k}^{m=4,5}\frac{z_{mj}z_{jk}z_{km}}{\omega_{THz}-\omega_{jk}+i\Gamma_{jk}}\left[\frac{N_m-N_j}{\omega_1-\omega_{mj}+i\Gamma_{mj}}+\frac{N_m-N_k}{-\omega_2+\omega_{mk}+i\Gamma_{mk}}\right] \qquad (2)\\
&+\frac{e^3}{\hbar^2\varepsilon_0}\sum_{j=1,2,3}\frac{z_{j5}z_{54}z_{4j}}{\omega_{THz}-\omega_{54}+i\Gamma_{54}}\left[\frac{N_5-N_j}{\omega_1-\omega_{5j}+i\Gamma_{5j}}+\frac{N_4-N_j}{-\omega_2+\omega_{4j}+i\Gamma_{4j}}\right]
\end{aligned}$$

Here j, k=1, 2, 3 and m=4, 5 represent the energy levels contributing the DFG nonlinearity. N_m is the population density distribution on level m. z_{mj}, ω_{mj}, and Γ_{mj} are the dipole matrix element, frequency, and broadening of the transition between levels m and j. ω_1, ω_2 , and ω_{THz} are the wave-vectors for the emitting wavelengths λ_1, λ_2, and λ_{THz}, respectively.

The increased transition broadening Γ_{mj} in the strong-coupled strain-balanced active region design will not affect $\chi^{(2)}$ significantly compared with the lattice matched design[17]. This is because the increased Γ_{mj} also requires an increased population inversion ΔN to satisfy the same threshold gain while $\chi^{(2)}$ is in proportional to ΔN. For our single core active region design, the gain is written as:

$$g(\omega)=\sum_{j,m}^{j\neq m}\frac{e^2\omega_{jm}^2}{c\varepsilon_0 n_{eff}\omega}\frac{z_{jm}^2\Gamma_{jm}}{\left(\hbar\omega_{mj}-\hbar\omega\right)^2+\Gamma_{mj}^2}\left(N_m-N_j\right) \qquad (3)$$

Here n_{eff} is the effective refractive index. The total gain $g(\omega)$ is obtained by sum all the possible transitions between different levels j and m (j, m=1, 2, ... $j\neq m$). Because the two wavelengths (λ_1 and λ_2) are defined on the two sides of the gain peak at λ_{peak}, the threshold condition for λ_1 which is shorter than λ_2 and has a lower free carrier absorption, can be expressed as:

$$g_{th}(\omega_1)=Tg_{th}(\omega_{peak})=\frac{\alpha_w+\alpha_m}{\Gamma} \qquad (4)$$

Here T is the ratio of the gain at λ_1 respect to the maximum gain at λ_{peak}. $T\approx$0.9-0.95 is estimated for the frequency spacing of 3-4 THz between λ_1 and λ_2. Γ is the modal confinement factor. Given a waveguide loss α_w= 1.2 cm^{-1} and mirror loss α_m= 1.8 cm^{-1} for a 4-mm long cavity with high-reflection (HR) coating, Γ_{mj} =15 meV for the mid-IR and THz transitions, modal confinement factor Γ= 60%, and also assuming all the lower laser levels 1-3 are depleted, ΔN=8×10^{14} and 6.5×10^{14} cm^{-3} were estimated. Therefore, $\chi^{(2)}$= (1.22-0.62i)×10^4 and (-0.2-1.04i)×10^4 pm/V are calculated for the two schemes (depicted in Fig. 1(b) and (c)) contributing to the nonlinearity. Thus a total $|\chi^{(2)}|$= 2.0×10^4 pm/V is obtained from the present design. Here, a transition broadening Γ_{jk}=5 meV for THz transitions is used in the calculation.

2. Mid-IR performance of a buried-ridge FP device based on n- substrate

A 4.9-mm long uncoated FP device on n-substrate is epilayer-down mounted and tested as a reference. The device exhibits a pulsed power up to 5.1 W with a threshold current density of 2.19 kA/cm^{-1}, and a CW power up to 1.6 W with a threshold current density of 2.5 kA/cm^{-1}, respectively, as shown in Figure 1S. The maximum WPE is 12.6% and 5%, respectively.

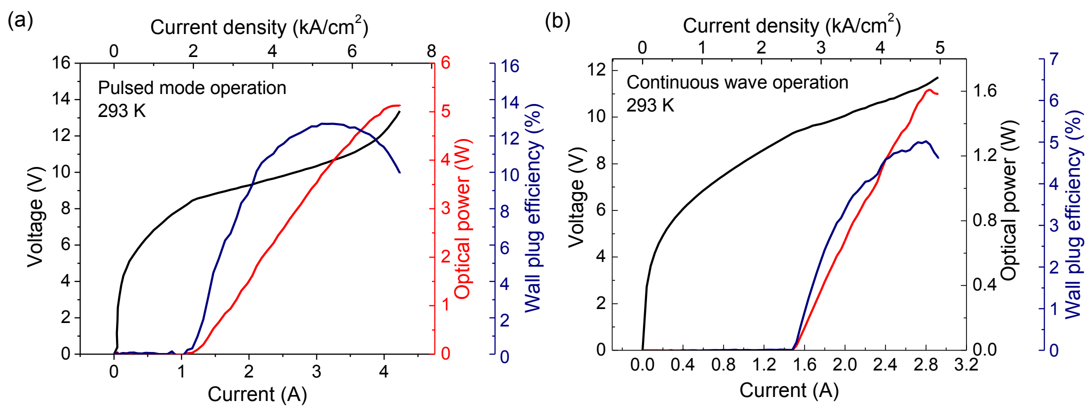

Fig. S1. *P-I-V* and wall plug efficiency characterizations of a 4.9-mm long uncoated FP device based on n- substrate in pulsed mode (a) and (b) CW operation at 293 K.

Reference:

1. Sirtori, C. et al. Resonant tunneling in quantum cascade lasers. IEEE J. Quantum Electron. 34, 1722–1729 (1998).